CORE
Metadata, citation and similar papers at core.ac.uk
Provided by St Andrews Research Repository

Room temperature strong coupling in a semiconductor microcavity with embedded AlGaAs quantum wells designed for polariton lasing

H. SUCHOMEL,[1,*] S. KREUTZER,[1] M. JÖRG,[1] S. BRODBECK,[1] M. PIECZARKA,[2] S. BETZOLD,[1] C. P. DIETRICH,[1,3] G. SĘK,[2] C. SCHNEIDER,[1] AND S. HÖFLING[1,3]

[1]*Technische Physik, Physikalisches Institut and Wilhelm Conrad Röntgen-Research Center for Complex Material Systems, Universität Würzburg, Am Hubland, 97074 Würzburg, Germany*
[2]*Laboratory for Optical Spectroscopy of Nanostructures, Department of Experimental Physics, Faculty of Fundamental Problems of Technology, Wrocław University of Technology, Wybrzeże Wyspiańskiego 27,Wrocław 50-370, Poland*
[3]*SUPA, School of Physics and Astronomy, University of St Andrews, St Andrews KY16 9SS, United Kingdom*
**holger.suchomel@physik.uni-wuerzburg.de*

Abstract: We report a systematic study of the temperature and excitation density behavior of an AlAs/AlGaAs, vertically emitting microcavity with embedded ternary $Al_{0.20}Ga_{0.80}As$/AlAs quantum wells in the strong coupling regime. Temperature-dependent photoluminescence measurements of the bare quantum wells indicate a crossover from the type-II indirect to the type-I direct transition. The resulting mixing of quantum well and barrier ground states in the conduction band leads to an estimated exciton binding energy systematically exceeding 25 meV. The formation of exciton-polaritons is evidenced in our quantum well microcavity via reflection measurements with Rabi splittings ranging from (13.93±0.15) meV at low temperature (30 K) to (8.58±0.40) meV at room temperature (300 K). Furthermore, the feasibility of polariton laser operation is demonstrated under non-resonant optical excitation conditions at 20 K and emission around 1.835 eV.

© 2017 Optical Society of America

OCIS codes: (190.5970) Semiconductor nonlinear optics including MGW; (140.3945) Microcavities; (160.3380) Laser materials.

References and links

1. C. Weisbuch, M. Nishioka, A. Ishikawa, and Y. Arakawa, "Observation of the coupled exciton-photon mode splitting in a semiconductor quantum microcavity," Phys. Rev. Lett. **69**(23), 3314-3317 (1992).
2. A. Imamoglu, R. J. Ram, S. Pau, and Y. Yamamoto, "Nonequilibrium condensates and lasers without inversion: Exciton-polariton lasers," Phys. Rev. A **53**(6), 4250-4253 (1996).
3. J. Kasprzak, M. Richard, S. Kundermann, A. Baas, P. Jeambrun, J. M. J. Keeling, F. M. Marchetti, M. H. Szymańska, R. André, J. L. Staehli, V. Savona, P. B. Littlewood, B. Deveaud, and L. Si Dang, "Bose-Einstein condensation of exciton polaritons," Nature **443**(7110), 409-414 (2006).
4. H. Deng, G. Weihs, C. Santori, J. Bloch, and Y. Yamamoto, "Condensation of semiconductor microcavity exciton polaritons," Science **298**(5591), 199-202 (2002).
5. H. Deng, G. Weihs, D. Snoke, J. Bloch, and Y. Yamamoto, "Polariton lasing vs. photon lasing in a semiconductor microcavity," Proc. Natl. Acad. Sci. U.S.A. **100**(26), 15318–15323 (2003).
6. R. Balili, V. Hartwell, D. Snoke, L. Pfeiffer, and K. West, "Bose-Einstein condensation of microcavity polaritons in a trap," Science **316**(5827), 1007-1010 (2007).
7. S. Christopoulos, G. Baldassarri Höger von Högersthal, A. J. D. Grundy, P. G. Lagoudakis, A. V. Kavokin, J. J. Baumberg, G. Christmann, R. Butté, E. Feltin, J.-F. Carlin, and N. Grandjean, "Room-temperature polariton lasing in semiconductor microcavities," Phys. Rev. Lett. **98**(12), 126405 (2007).
8. Y.-Y. Lai, Y.-P. Lan, and T.-C. Lu, "High-Temperature Polariton Lasing in a Strongly Coupled ZnO Microcavity," Appl. Phys. Express. **5**(8), 082801 (2012).
9. S. Kéna-Cohen, and S. R. Forrest, "Room-temperature polariton lasing in an organic single-crystal microcavity," Nat. Photon. **4**(6), 371-375 (2010).

10. S. I. Tsintzos, P. G. Savvidis, G. Deligeorgis, Z. Hatzopoulos, and N. T. Pelekanos, "Room temperature GaAs exciton-polariton light emitting diode," Appl. Phys. Lett. **94**(7), 071109 (2009).
11. C. Schneider, P. Gold, S. Reitzenstein, S. Höfling, and M. Kamp, "Quantum dot micropillar cavities with quality factors exceeding 250.000," Appl. Phys. B **122**(1), 19 (2016).
12. C. Schneider, A. Rahimi-Iman, N. Y. Kim, J. Fischer, I. G. Savenko, M. Amthor, M. Lermer, A. Wolf, L. Worschech, V. D. Kulakovskii, I. A. Shelykh, M. Kamp, S. Reitzenstein, A. Forchel, Y. Yamamoto, and S. Höfling, "An electrically pumped polariton laser," Nature **497**(7449), 348-352 (2013).
13. P. Bhattacharya, B. Xiao, A. Das, S. Bhowmick, and J. Heo, "Solid State Electrically Injected Exciton-Polariton Laser," Phys. Rev. Lett. **110**(20), 206403 (2013).
14. T. Jacqmin, I. Carusotto, I. Sagnes, M. Abbarchi, D. D. Solnyshkov, G. Malpuech, E. Galopin, A. Lemaître, J. Bloch, and A. Amo, "Direct Observation of Dirac Cones and a Flatband in a Honeycomb Lattice for Polaritons," Phys. Rev. Lett. **112**(11), 116402 (2014).
15. K. Winkler, J. Fischer, A. Schade, M. Amthor, R. Dall, J. Geßler, M. Emmerling, E. A. Ostrovskaya, M. Kamp, C. Schneider, and S. Höfling, "A polariton condensate in a photonic crystal potential landscape," New J. Phys. **17**, 23001 (2015).
16. C. Schneider, K. Winkler, M. D. Fraser, M. Kamp, Y. Yamamoto, E. A. Ostrovskaya, and S. Höfling, "Exciton-polariton trapping and potential landscape engineering," Reports Prog. Phys. **80**(1), 16503 (2017).
17. J.-S. Tempel, F. Veit, M. Assmann, L. E. Kreilkamp, S. Höfling, M. Kamp, A. Forchel, and M. Bayer, "Temperature dependence of pulsed polariton lasing in a GaAs microcavity," New J. Phys. **14**, 083014 (2012).
18. L. C. Andreani, and A. Pasquarello, "Accurate theory of excitons in GaAs-$Ga_{1-x}Al_xAs$ quantum wells," Phys. Rev. B **42**(14), 8928-8938 (1990).
19. J. B. Khurgin, "Excitonic radius in the cavity polariton in the regime of very strong coupling," Solid State Commun. **117**(5), 307-310 (2001).
20. M. Pieczarka, P. Podemski, A. Musial, K. Ryczko, G. Sęk, J. Misiewicz, F. Langer, S. Höfling, M. Kamp, and A. Forchel, "GaAs-Based Quantum Well Exciton-Polaritons beyond 1 μm," Acta. Phys. Pol. A **124**(5), 817-820 (2013).
21. H. Zhang, N. Y. Kim, Y. Yamamoto, and N. Na, "Very strong coupling in GaAs-based optical microcavities," Phys. Rev. B **87**(11), 115303 (2013).
22. N. Chand, T. Henderson, J. Klem, W. T. Masselink, R. Fischer, Y.-C. Chang, and H. Morkoĉ, "Comprehensive analysis of Si-doped $Al_xGa_{1-x}As$ (x=0 to 1): Theory and experiments," Phys. Rev. B **30**(8), 4481-4492 (1984).
23. A. J. SpringThorpe, F. D. King, and A. Becke, "Te- and Ge-doping studies in $Ga_{1-x}Al_xAs$," J. Electron. Mater. **4**(1), 101-118 (1975).
24. P. Pearah, W. Masselink, J. Klem, T. Henderson, H. Morkoç, C. Litton, and D. Reynolds, "Low-temperature optical absorption in $Al_xGa_{1-x}As$ grown by molecular-beam epitaxy," Phys. Rev. B **32**(6), 3857-3862 (1985).
25. M. Z. Baten, P. Bhattacharya, T. Frost, S. Deshpande, A. Das, D. Lubyshev, J. M. Fastenau, and A. W. K. Liu, "GaAs-based high temperature electrically pumped polariton laser," Appl. Phys. Lett. **104**(23), 231119 (2014).
26. B. Deveaud, "Comment on "Room Temperature Electrically Injected Polariton Laser"," Phys. Rev. Lett. **117**(2), 029701 (2016).
27. P. Bhattacharya, T. Frost, S. Deshpande, M. Z. Baten, A. Hazari, and A. Das, "Comment on "Room Temperature Electrically Injected Polariton Laser" Reply," Phys. Rev. Lett. **117**(2), 029702 (2016).
28. P. Tsotsis, P. S. Eldridge, T. Gao, S. I. Tsintzos, Z. Hatzopoulos, and P. G. Savvidis, "Lasing threshold doubling at the crossover from strong to weak coupling regime in GaAs microcavity," New J. Phys. **14**, 023060 (2012).
29. S. Dufferwiel, S. Schwarz, F. Withers, A. A. P. Trichet, F. Li, M. Sich, O. Del Pozo-Zamudio, C. Clark, A. Nalitov, D. D. Solnyshkov, G. Malpuech, K. S. Novoselov, J. M. Smith, M. S. Skolnick, D. N. Krizhanovskii, and A. I. Tartakovskii, "Exciton–polaritons in van der Waals heterostructures embedded in tunable microcavities," Nat. Commun. **6**, 8579 (2015).
30. N. Lundt, S. Klembt, E. Cherotchenko, O. Iff, A. V. Nalitov, M. Klaas, S. Betzold, C. P. Dietrich, A. V. Kavokin, S. Höfling, and C. Schneider, "Room temperature Tamm-Plasmon Exciton-Polaritons with a WSe2 monolayer," Nat. Commun. **7**, 13328 (2016).
31. D. M. Shcherbakova, and V. V. Verkhusha, "Near-infrared fluorescent proteins for multicolor in vivo imaging," Nat. Methods **10**(8), 751-754 (2013).
32. J. Singh, and K. K. Bajaj, "Role of interface roughness and alloy disorder in photoluminescence in quantum-well structures," J. Appl. Phys. **57**(12), 5433-5437 (1985).
33. I. Vurgaftman, J. R. Meyer, L. R. Ram-Mohan, "Band parameters for III-V compound semiconductors and their alloys," J. Appl. Phys. **89**(11), 5815-5875 (2001).
34. R. Cingolani, L. Baldassarre, M. Ferrara, M. Lugarà, and K. Ploog, "Type-I–type-II transition in ultra-short-period GaAs/AlAs superlattices," Phys. Rev. B **40**(9), 6101-6107 (1989).
35. D. S. Jiang, H. Jung, and K. Ploog, "Temperature dependence of photoluminescence from GaAs single and multiple quantum-well heterostructures grown by molecular-beam epitaxy," J. Appl. Phys. **64**(3), 1371-1377 (1988).
36. V. Savona, L.C. Andreani, P. Schwendimann, and A. Quattropani, "Quantum well excitons in semiconductor microcavities: Unified treatment of weak and strong coupling regimes," Solid State Commun. **93**(9), 733-739 (1995).
37. D. Gammon, S. Rudin, T. L. Reinecke, D. S. Katzer, and C. S. Kyono, "Phonon broadening of excitons in GaAs/$Al_xGa_{1-x}As$ quantum wells," Phys. Rev. B **51**(23), 16785-16789 (1995).

38. S. Adachi, "GaAs, AlAs, and $Al_xGa_{1-x}As$: Material parameters for use in research and device applications," J. Appl. Phys. **58**(3), R1-R29 (1985).
39. A. R. Pratt, T. Takamori, and T. Kamijoh, "Temperature dependence of the cavity-polariton mode splitting in a semiconductor microcavity," Phys. Rev. B **58**(15), 9656-9658 (1998).
40. J.-S. Tempel, F. Veit, M. Assmann, L. E. Kreilkamp, A. Rahimi-Iman, A. Löffler, S. Höfling, S. Reitzenstein, L. Worschech, A. Forchel, and M. Bayer, "Characterization of two-threshold behavior of the emission from a GaAs microcavity," Phys. Rev. B **85**(7), 075318 (2012).
41. D. Bajoni, P. Senellart, A. Lemaître, and J. Bloch, "Photon lasing in GaAs microcavity: Similarities with a polariton condensate," Phys. Rev. B **76**(20), 201305(R) (2007).
42. R. Butté, J. Levrat, G. Christmann, E. Feltin, J.-F. Carlin, and N. Grandjean, "Phase diagram of a polariton laser from cryogenic to room temperature," Phys. Rev. B **80**(23), 233301 (2009).

1. Introduction

Strong coupling between microcavity photons and quantum well (QW) excitons leads to the generation of new quasi-particles with a hybrid light-matter character named exciton-polaritons (polaritons). Since the first observation of polaritons in a GaAs/AlGaAs based semiconductor microcavity [1] it was possible to demonstrate strong coupling and polariton lasing [2,3] in many different semiconductor materials from low temperature [3-6] up to room temperature [7-10]. Nevertheless, the GaAs/AlGaAs material platform remains the workhorse material in polaritonics, due to its unprecedented material quality provided by state of the art molecular beam epitaxy. Due to the very small lattice mismatch between GaAs and AlAs, it is relatively easy to handle, and ideal for the fabrication of semiconductor microcavities with very high quality [11]. Moreover, it is well-established for the growth of doped structures and for complex processing technologies necessary for advanced spectroscopic experiments like electrically driven polariton lasing [12,13] or potential landscape engineering [14-16]. On the other hand, using GaAs QWs, polariton lasing is limited to temperatures below ~ 70 K [17] since the exciton binding energy is of the order of ~ 10 meV [18] which leads to a thermal dissociation of excitons above these temperatures.

There have been efforts to realize samples with increased exciton binding energy based on GaAs in order to extend the temperature range of existing polariton devices. Increasing the light-matter coupling strength to be comparable to the binding energy and thus reaching the regime of very strong coupling [19,20] may stabilize excitons in GaAs even at room temperature [21]. In another approach, changing the QW material to AlGaAs could drastically increase the exciton binding energy which shows a sharp increase in bulk $Al_xGa_{1-x}As$ for $x > 0.3$ similar to the increase of donor activation energy in this material [22-24]. Mixing of Γ-valley electrons with the X- and L-valley leads to an increase of the electron effective mass which, in turn, should lead to an increase of the exciton binding energy that is proportional to its effective mass. Polariton lasing at 155 K was recently claimed for a sample with an $Al_{0.31}Ga_{0.69}As/Al_{0.41}Ga_{0.59}As$ QW [25], but the unconventional microcavity geometry in a lateral configuration, which is highly unsuitable for advanced spectroscopic experiments, led to an open debate on the conclusions that were drawn based on measurements on such samples [26,27].

Besides the limitation to low temperature operation of GaAs QW based polariton microcavities, the emission energy of such structures has only been varied by adjusting the QW width as well as the Al-concentration of the barrier material. Therefore, the emission energy typically ranges from 1.61 eV [4] to 1.54 eV [28]. The Al-concentration of the QW itself can be used as another adjusting parameter by changing the QW material to AlGaAs which opens the way to a completely new energy range for GaAs/AlGaAs based polariton systems well up to ~ 2.0 eV. Therefore, those structures are highly suitable for strong coupling with commonly used transition metal dichalcogenide monolayers [29,30] and fluorescent proteins [31] in hybrid cavity approaches.

Here, we investigate $Al_{0.20}Ga_{0.80}As/AlAs$ QWs in a standard, vertically emitting microcavity. Calculations of the band diagram and temperature-dependent photoluminescence measurements of the bare quantum wells indicate a crossover from the type-II indirect to the

type-I direct transition as well as exciton binding energies exceeding 25 meV, being necessary for stable excitons at room temperature. Strong coupling is observed over the whole temperature range from 20 K to 300 K. Furthermore, we performed power-dependent photoluminescence (PL) measurements under non-resonant excitation conditions at low temperature to test the structure for polariton lasing.

2. Sample structure

2.1 Sample growth

The microcavity structure was grown by molecular beam epitaxy on a nominally undoped (001) GaAs substrate. It consists of a λ/2-AlAs cavity surrounded by AlAs/$Al_{0.40}Ga_{0.60}As$ distributed Bragg reflectors (DBRs). The bottom (top) reflector consists of 28 (24) mirror pairs including 3 nm GaAs smoothing layers after each mirror pair in the local minimum of the electromagnetic field. Three stacks, each consisting of four $Al_{0.20}Ga_{0.80}As$ QWs with 9 nm width and separated by 4 nm AlAs barriers, are placed in the center of the cavity and the first mirror pair in the bottom (top) Bragg reflector. The layer structure is schematically depicted in Fig. 1(a) together with a scanning electron microscope image of the cavity region highlighting the embedded QWs in Fig. 1(b). The theoretical cavity Q-factor was extracted from transfer matrix calculations and amounts to ~ 6000. The bare QW properties were measured on a piece where the upper DBR was removed by reactive ion etching. Figure 1(c) shows the low excitation power PL (~ 0.5 $W \cdot cm^{-2}$) of the QWs at ~ 20 K under cw-excitation at 532 nm with a frequency-doubled Nd:YAG laser. The spot size is determined to be ~ 150 µm. Due to interface and composition fluctuations, the QWs exhibit a linewidth (full width at half maximum, FWHM) of 6.5 meV [32].

2.2 Band diagram and quantum well characteristics

The well-established band parameters of the GaAs/AlGaAs material platform allow an accurate calculation of the band diagram and the energy states of the investigated QW system [33]. The band diagram and the respective calculated ground states of the different bands are shown in Fig. 2(a) at 5 K to provide a better understanding of the system. The Γ-band (solid black line), the X-band (solid red line) and the heavy hole valence band (solid orange line) are shown. Furthermore, the QW ground states of the heavy holes in the valence band (hh1)

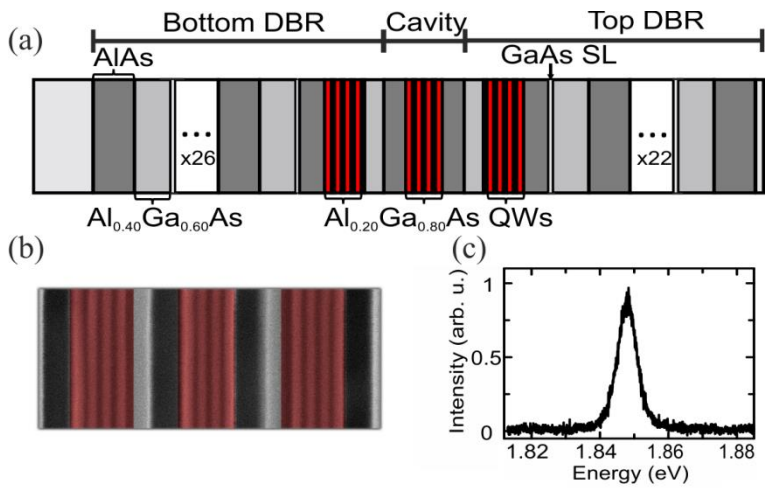

Fig. 1. (a) Schematic drawing of the layer structure of the investigated microcavity. (b) Scanning electron microscope image of the cavity region of the grown structure highlighting the three stacks of four $Al_{0.20}Ga_{0.80}As$ quantum wells (red). (c) Low excitation power photoluminescence at 20 K of the 9 nm $Al_{0.20}Ga_{0.80}As$ quantum well embedded in AlAs barriers.

and the electrons in the conduction band (e1) calculated in the effective mass approximation are indicated by the dashed lines inside the $Al_{0.20}Ga_{0.80}As$ QW region. Note that the AlAs barrier material acts as an additional QW for the X-band electrons. Therefore, the X-band energy states are also quantized in which the X_Z state (red dashed line) with its *k*-vector perpendicular to the QW plane provides the ground state. In this low-temperature case, the type-II indirect transition from the quantized X-valley state in the barrier (X_Z) to the first heavy hole QW energy state (hh1) is the lowest energy transition. With increasing temperature the band edges and therefore the energy states shift according to their Varshni-coefficients, resulting in a crossover to the type-I direct transition as lowest energy transition at approximately 70 K, Fig. 2(b). That means the lowest quantized energy state of the AlGaAs QWs in the conduction band corresponds to the conduction band ground state above the crossover temperature.

Due to the reduced overlap of the electron and hole wave functions localized in the barrier and the QW material the type-II indirect transition (X_Z-hh1) is less probable than the type-I direct transition (e1-hh1). Therefore, although the type-II indirect transition corresponds to the lowest energy transition below 70 K the type-I direct transition (e1-hh1) typically dominates the PL spectrum [34]. To verify this, we tracked the temperature-

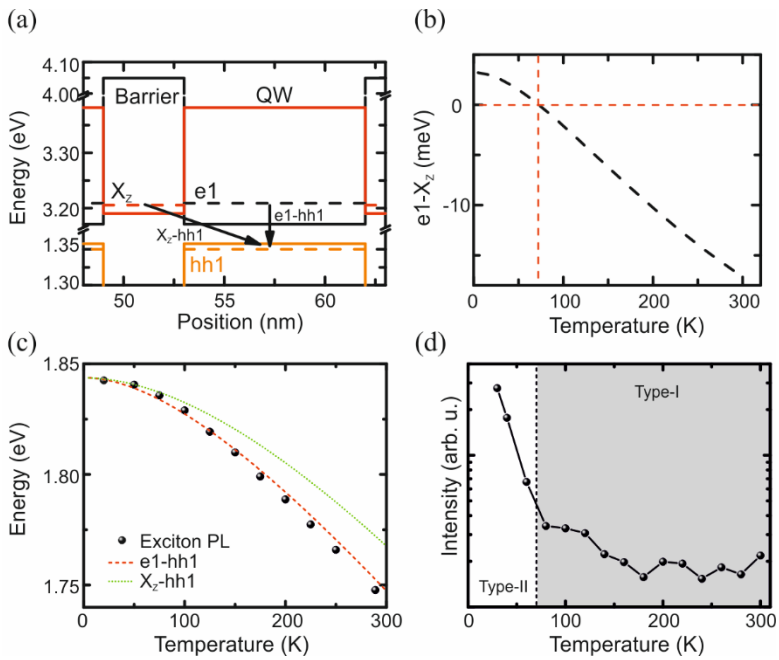

Fig. 2. (a) Calculated band diagram at low temperature (5 K) for the grown quantum wells. Shown are the Γ-band (solid black line), the X-band (solid red line) and the valence band (solid orange line). The arrows indicate the type-II indirect transition from the quantized X-valley state in the barrier (X_Z) to the first heavy hole quantum well energy state (hh1) and the direct transition from the first Γ-valley state inside the quantum well to hh1. (b) Calculated energy difference between e1 and X_Z as a function of temperature. Above ~ 70 K the quantum well system is direct. (c) Temperature-dependent photoluminescence of the bare exciton at low excitation power (~ 0.5 $W \cdot cm^{-2}$), together with the calculated trend of the type-II indirect (green dotted line) and the type-I direct (red dashed line) transition. The calculated lines are shifted to fit the experimental values at low temperature. (d) Temperature-dependent intensity of the bare exciton photoluminescence, while keeping the excitation power constant at non-resonant excitation. The deviation from the decreasing photoluminescence intensity with increasing temperature around 70 K indicates the crossover from the type-II indirect to the type-I direct transition, due to charge transfer between the valleys. Note that the direct transition was probes over the whole temperature range.

dependent energy position of the PL peak in Fig. 2(c), which follows the calculated temperature-dependence of the type-I direct transition in the whole temperature range between low (20 K) and room temperature (300 K).

The type-II indirect transition character of the sample can be seen around the crossover of the conduction band ground state from X_Z to e1 at around 70 K in the temperature-dependent PL intensity, Fig. 2(d). We kept the excitation power constant and excited the sample non-resonantly at 532 nm with a frequency-doubled Nd:YAG laser, while probing the photoluminescence intensity as a function of temperature. The PL intensity typically decreases with increasing temperature due to non-radiative recombination mechanisms [35]. Therefore, in Fig. 2(d) one would expect a continuous decrease of the integrated PL intensity. However, a strong deviation from this behavior is seen in the temperature range around 70 K where we expect the crossover from the type-II indirect to the type-I direct transition. We believe that the carrier trapped in the barrier material below 70 K start to transfer into the QW around the crossover. In turn, these additional carriers temporally counteract the decreasing PL intensity with increasing temperature [34]. We like to emphasize that the type-I direct transition was probed over the whole temperature range. However, the deviation from the decreasing PL intensity with increasing temperature is only an indication for a type-II to type-I transition. But we believe that the occurrence at nearly the same temperature as the calculated transition is a strong indication for an interplay between the X-valley of the barrier material and the Γ–valley of the QW material, necessary for intervalley mixing as proposed by Pearah et al. [24].

There is an almost constant offset between the energy of the low power PL peak and the calculated e1-hh1 transition energy without Coulomb interaction at all temperatures of (48±10) meV which we identify as the exciton binding energy. This value is in good agreement with literature [24], considering the spatial confinement of the QW structure. The error range is due to the uncertainty of Al-concentration and thickness of the QWs which were determined by X-ray diffraction measurements. In a first simple effective mass approximation the exciton binding energy E_B is given by

$$E_B = \left(\frac{m^*}{m_0}\right)\frac{R_y}{\varepsilon^2}, \tag{1}$$

where m^* is the effective mass of the conduction-band electrons, m_0 the free-electron mass, ε the static dielectric constant of the semiconductor and R_y = 13.6 eV the Rydberg energy. Increasing the Al-concentration x of the quantum well material leads to an increase of m^* and to a decrease of ε. Therefore, according to Eq. (1), an increase of x leads to a linear increase of the exciton binding energy E_B. However, in the case where multiple valleys of the quantum well and the barrier conduction band has to be considered, the mixing of those further increases the binding energy, due to a non-linear increase of the overall effective mass [24]. A detailed treatment of a multivalley effective mass model can be found in [22]. The determined estimation for the exciton binding energy exceeds the value necessary for room temperature stable QW excitons. Therefore, our investigated AlGaAs-based microcavity system is probably suitable to promote polariton formation at high temperatures.

In terms of photoluminescence intensity the design of the band diagram around the crossover is unfavorable, since the indirect transition competes with the direct one. On the other hand, the proximity of both transitions is necessary to achieve a sufficient intervalley mixing as proposed by Pearah et al. [24]. In our structure the band diagram is designed in the way that the energy difference between the electronic states in the conduction band barrier and quantum well is always less than the thermal energy. Therefore, we expect a sufficient intervalley mixing over the whole temperature range. However, the structure can easily be optimized for room temperature, simply by adjusting the width of the barrier and the QW but also shifting the emission energy.

3. Results and discussion

3.1 Temperature-dependent determination of the Rabi splitting

As a first step, we confirm that strong coupling persists at room temperature by measuring the anti-crossing of QW exciton and cavity photon modes in temperature-dependent white-light reflection measurements. Due to the layer thickness gradient along the wafer introduced during sample growth (~ 20 meV/mm), it is possible to tune the cavity resonance through the exciton energy by varying the radial position of the light spot over the planar wafer. The Q-factor was artificially reduced in these measurements by removing approximately 10 mirror pairs from the top DBR via reactive ion etching to improve the contrast of the absorption resonances. Figures 3(a) and 3(b) show reflection spectra at various positions obtained at 30 K (a) and 300 K (b). The respective spectra are shifted vertically for clarity while the photon-exciton detuning is changed from far red (bottom) to far blue (top). The arrows indicate the position of the individual polariton branches which we identify as the lower (LP), middle (MP) and the upper (UP) polariton. Clear anti-crossings between the LP and the MP as well as the MP and UP are visible at low- (30 K) and room temperature (300 K) as the cavity mode is tuned through the heavy hole- and light hole-exciton energies of the AlGaAs QWs. Rabi splittings $\hbar\Omega$ are determined as the minimal difference between the fitted energies of the reflectivity dips, that means MP-LP as well as UP-MP, which are plotted in Figs. 3(c) and (d) for measurements at 30 K (c) and at 300 K (d). The horizontal dashed lines mark the

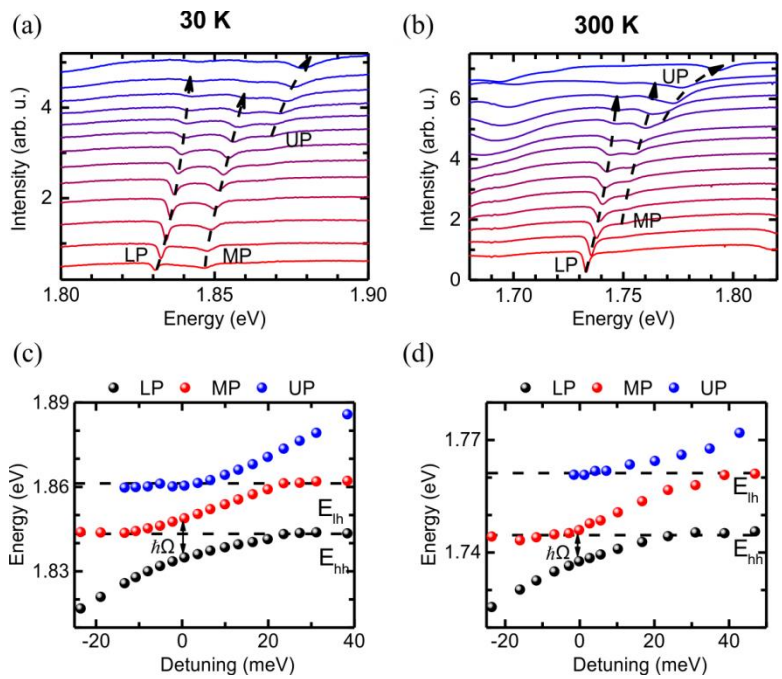

Fig. 3. White light reflection measurements of the planar microcavity sample at different positions on the wafer at 30 K (a) and 300 K (b). The spectra are shifted vertically such that the photon-exciton detuning shifts from red (bottom) to blue (top). Arrows indicate the position of the lower (LP), middle (MP) and the upper (UP) polariton branches. Extracted energies of the different polariton branches at 30 K (c) and 300 K (d). Clear anti-crossings between the LP and the MP as well as the MP and the UP are visible at both temperatures. Dashed lines mark the energy positions of the uncoupled heavy hole (E_{hh}) and the light hole (E_{lh}) excitons.

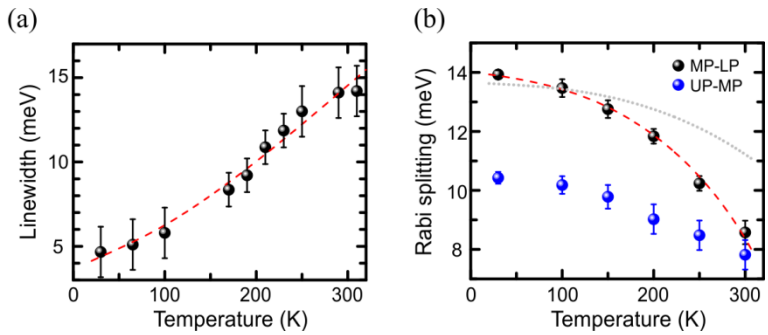

Fig. 4. (a) Temperature-dependent linewidth of the heavy hole QW exciton together with the fitted exponential function according to Eq. (4) (dashed red line). (b) Temperature-dependent Rabi-splitting extracted from white-light reflection measurements. The dashed red line represents a fit to the temperature-dependent heavy hole Rabi splitting using Eq. (3) while the dotted grey line represents a fit using the standard coupled oscillator approach, Eq. (2).

measured energy position of the uncoupled heavy hole exciton (E_{hh}) and the light hole exciton (E_{lh}). The heavy and light hole exciton are energetically separated by more than ~ 20 meV. Therefore, the coupling of both excitons to the cavity mode can be considered to be independent from each other. The detuning was estimated by tracking the energy of an additional reflectivity minimum outside the stop band which shifts parallel to the bare cavity mode. On the one hand, the heavy hole Rabi splitting between the MP and the LP at 30 K amounts to $\hbar\Omega$ = (13.93±0.15) meV, while we extract a value of $\hbar\Omega$ = (8.58±0.40) meV at 300 K. On the other hand, the light hole Rabi splitting between the UP and the MP at 30 K (300 K) amounts to $\hbar\Omega$ = (10.43±0.20) meV (7.82±0.50 meV). We like to note that we attribute both crossings to the coupling between the cavity mode and the respective direct excitons in the whole temperature range, due to their significant higher oscillator strength.

The Rabi splitting can be expressed in terms of the linewidths (FWHM) of the cavity photon γ_C and the respective QW exciton γ_X, as well as the coupling strength V between the cavity photon and the QW exciton. Here, we note that different measurement techniques yield different splittings between the polariton branches [36]. This effect becomes particularly dominant in the presence of strong emitter dephasing and finite reflectivity of the cavity, which leads to strong deviations from the standard coupled oscillator approach, including one cavity and one exciton mode as a system of two damped harmonic oscillators, coupled by the matrix element V [30]. In the standard coupled oscillator approach the Rabi splitting can be written as

$$\hbar\Omega = \sqrt{4V^2 - \frac{1}{4}(\gamma_C - \gamma_X)^2}, \tag{2}$$

while in the case of reflectivity measurements the Rabi splitting reads in the high reflectivity limit

$$\hbar\Omega_R = 2\sqrt{\sqrt{V^4\left(1+\frac{2\gamma_X}{\gamma_C}\right)^2 + \frac{1}{2}V^2\gamma_X^2\left(1+\frac{\gamma_X}{\gamma_C}\right)} - 2V^2\frac{\gamma_X}{\gamma_C} - \frac{\gamma_X^2}{4}}. \tag{3}$$

The whole temperature-dependence of the Rabi splitting $\hbar\Omega(T)$ can then be described by taking into account the temperature-dependent linewidth of the exciton [37]

$$\gamma_X(T) = \gamma_{inh} + \gamma_{AC}T + \gamma_{LO}\left(\exp\left\{\frac{\hbar\Omega_{LO}}{k_BT}\right\} - 1\right)^{-1}, \tag{4}$$

while the coupling strength and the intrinsic cavity photon linewidth can be assumed to be temperature-independent. The parameter γ_{inh} in Eq. (4) describes the low-temperature inhomogeneous broadening due to interface roughness, while γ_{AC} and γ_{LO} describe the interaction strength with acoustic and longitudinal optical (LO) phonons. The material constant $\hbar\Omega_{LO}$ specifies the LO-phonon energy which amounts to 37.4 meV in the used QWs [38]. To determine $\gamma_X(T)$, we performed temperature-dependent white-light reflectivity measurements on the microcavity sample after removing the full top DBR via reactive ion etching such that the system is in the weak coupling regime. The determined temperature-dependent linewidth of the heavy hole exciton is plotted in Fig. 4(a). Fitting the obtained data
with Eq. (4) yields γ_{inh} = (4.09±0.45) meV, γ_{AC} = (29.7±5.0) µeV/K and γ_{LO} = (11.8±4.0) meV, red dashed line in Fig. 4(a). The broadening due to acoustic phonons is negligible [10,37,39] whereas the contribution due to LO phonons is in a good agreement with literature [37]. The linewidth of the cavity photon was measured directly on the unetched microcavity sample far off resonance and amounts to γ_C = (2.05±0.10) meV. Discrepancy between the theoretical Q-factor value and the experimental one is mainly due to the intrinsic sample gradient, limiting the measurable Q-factor, and is not reflecting the high-quality of the DBRs and the cavity. Furthermore, the sample gradient leads to increased losses of photons perpendicular to the growth direction which could be compensated by guiding the photons within etched micropillar structures. Repeating the detuning-dependent reflection measurements as discussed in Fig. 3 for different temperatures, yields the temperature-dependent Rabi splitting plotted in Fig. 4(b). The heavy hole Rabi splitting can be fitted using Eq. (3) with only the coupling strength V as a free fitting parameter. The red dashed line in Fig. 4(b) represents the fitted temperature-dependent heavy hole Rabi splitting using the fitted values from Fig. 4(a) for $\gamma_X(T)$ and the measured photon linewidth. The heavy hole coupling strength amounts to V = (7.10±0.20) meV. The provided theory gives a very good agreement with the measured values for the Rabi splitting over the whole temperature range. On the other hand, the grey dotted line in Fig. 4(b) represents a fit using the standard coupled oscillator approach according to Eq. (2) and shows a strong deviation from the experimental data.

3.2 Power-dependent photoluminescence

Power-dependent PL emission of the unetched microcavity sample was investigated via momentum-resolved spectroscopy. The sample was mounted in a helium flow cryostat to cool it down to a temperature of ~ 20 K. A pulsed optical parametric oscillator (OPO) laser with a spot size of ~ 5 µm at a repetition rate of 20 Hz and with a pulse length of about ~ 8 ns was used for excitation. The laser energy was tuned to the reflectance minimum of the first high-energy Bragg mode around 1.943 eV. A longpass filter with a cut-off energy of 1.907 eV was placed in front of the spectrometer to filter any scattered light from the laser. Figure 5(a) depicts the resulting spectra at different excitation powers. Under moderate excitation conditions of ~ 21.8 W·cm^{-2} per pulse, which corresponds to an average exciton density per pulse of ~ 1.4·10^{9} cm^{-2}, a parabolic dispersion which flattens to higher $k_{||}$-vectors is observed, which we identify as the lower polariton branch (LP). For the estimated average exciton density per pulse we assume a coupling efficiency of the microscope objective of T_{Obj} = 0.80, a transmission of the cryostat window of T_{Cryo} = 0.90, and furthermore a sample reflectivity of R_{Sample} = 0.30 at the pumping wavelength extracted from low-temperature reflectivity measurements. Furthermore, we assume 1% absorption per QW. The spectrum was fitted using the standard coupled oscillator model by coupling the cavity mode with the heavy hole exciton. Taking fixed the experimental values for the exciton energy (1.8425 eV) and the Rabi splitting (13.9 meV), the cavity mode energy remains the only free fitting parameter. In this low temperature case, that means small emitter dephasing, Eq. (2) and (3) hardly differ from each other. This is why the experimental value taken from reflectivity measurements can be used as a fixed input parameter to fit the dispersion. Data fitting yields a heavy hole

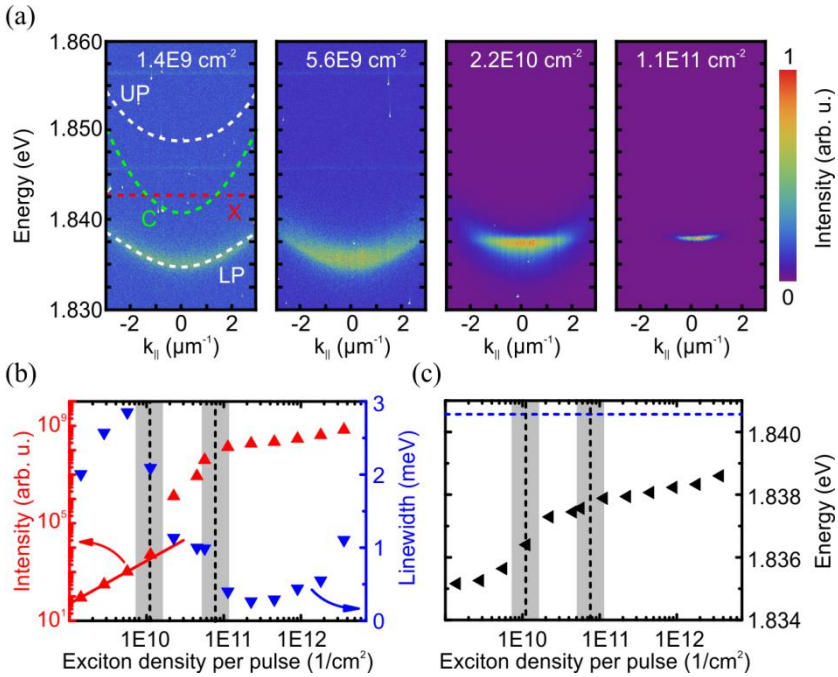

Fig. 5. (a) Momentum-resolved photoluminescence spectra at different excitation powers. The low power spectrum was fitted using the standard coupled oscillator model by coupling the cavity mode with the heavy hole exciton. White dashed lines indicate the lower (LP) and upper (UP) polariton branch, as well as the uncoupled exciton (X, red) and photon mode (C, green). (b) Power-dependent emission intensity and linewidth (FWHM), extracted from the momentum resolved spectra around zero $k_{||} \sim 0$. (c) Corresponding power-dependent emission energy. The vertical black line indicates the threshold, while the horizontal blue dashed line indicates the energy of the uncoupled cavity mode.

photon-exciton detuning of $\delta \sim$ -2.0 meV. With increasing pump power, polariton lasing takes place which is manifested by a massive occupation of the lowest polariton energy state. To analyze the power-dependent PL emission in more detail, we extracted spectra around $k_{||}$ = (0.00±0.15) μm^{-1} from the momentum resolved spectra. Figure 5(b) depicts the emission intensity as well as the evolution of the linewidth as a function of the pump power, Fig. 5(c) depicts the corresponding power-dependent emission energy as well as the bare cavity energy position (blue dashed line). With increasing pump power the integrated emission intensity shows a non-linear increase from which we extract a threshold average exciton density per pulse of ~ 1.1·10^{10} cm^{-2}. The non-linear increase is accompanied by a distinct linewidth drop and a continuing blue shift of the emission energy, which are typical indications of polariton lasing [40]. Increasing the pump power further leads to the formation of a second threshold attributed to the onset of photon lasing at an average exciton density per pulse of ~ 8·10^{10} cm^{-2}. The offset between the uncoupled cavity mode, which is marked by the blue dashed line in Fig. 5(c), and the actual photon lasing can be attributed to an incompletely blueshift [41]. Another possible explanation could be that the photon laser mode is pinned to a maximum of the modal gain above the Mott density.

Besides strong coupling between the cavity photon and the quantum well exciton, polariton lasing requires a mean occupation of the lower polariton branch ground state exceeding unity, leading to a non-linear increase of the ground state population due to stimulated scattering processes as a function of pump power. In the investigated microcavity structure the Q-factor limits the lower polariton lifetime around $k_{||} \sim 0$ for negative photon-exciton detunings to less than 3.5 ps which hinders the built up of a sufficient ground state population at elevated temperatures. With increasing temperature, the thermal escape of polaritons from the energy

trap formed in $k_{||}$-space by the lower polariton branch has to be compensated by increasing the negative photon-exciton detuning [42]. This, in turn, leads to a further decrease of the polariton lifetime. Therefore, we believe that by increasing the Q-factor of the GaAs/AlGaAs based microcavity structure, and thereby the polariton lifetime, polariton lasing at significant higher temperatures are within reach.

4. Conclusion

To conclude, in this letter we investigate the temperature-dependent Rabi splitting of an AlGaAs QW-based, vertically emitting microcavity. Significant anti-crossings of the cavity mode with heavy hole- and light hole-excitons are observed even at room temperature. The temperature-dependence of the Rabi splitting is well reproduced by the original model of Savona et al. [36], while the standard coupled oscillator model breaks down for increased temperature induced emitter dephasing. The band diagram of the cavity structure is designed around the crossover from the type-II indirect to the type-I direct transition. Therefore, the structure possible enables to exploit multivalley mixing between the X-valley electrons of the AlAs barrier and the Γ-valley electrons of the AlGaAs QWs in the conduction band which results in an estimated exciton binding energy exceeding 25 meV, necessary for room temperature stable excitons. Furthermore, we performed power-dependent photoluminescence measurements under non-resonant excitation conditions to test the structure for polariton lasing. Clear cut polariton lasing could be demonstrated at cryogenic temperatures (20 K) and an emission energy of 1.835 eV. We believe that the realization of polariton lasing in a GaAs/AlGaAs based microcavity structure opens the way to a wide variation of the polariton emission energy by adjusting the Al-concentration of the AlGaAs QWs.

Acknowledgments

The authors thank A. Wolf and M. Wagenbrenner for assistance during sample growth and fabrication. This work was supported by the State of Bavaria.